Single-stack multilayer infrared mirrors with selectable higher-order interference peaks

R. MEISELS,[1] F. KUCHAR,[1] J. MANARA,[2] M. ARDUINI,[2] U. SCHULZ,[3] J. O. PETERS,[4] T. M. GARTNER,[4,#] C. MITTERER,[5] AND O. PARIS[1,*]

[1]*Chair of Physics, Department Physics, Mechanics and Electrical Engineering, Montanuniversität Leoben, Leoben, AUSTRIA*
[2] *Center for Applied Energy Research e.V., Würzburg, GERMANY*
[3]*Deutsches Zentrum für Luft und Raumfahrt, Köln, GERMANY*
[4]*Lufthansa Technik AG, Hamburg, GERMANY*
[5]*Department of Materials Science, Montanuniversität Leoben, Leoben, AUSTRIA*
 # Present address: misc GmbH, Hamburg, GERMANY
** Corresponding author: oskar.paris@unileoben.ac.at*

Abstract: A concept for the design of single-stack multilayer mirrors with multiple reflection peaks is presented. Its realization in the infrared is demonstrated by the sputter deposition of TiO_2/Al_2O_3 bilayers on sapphire and HastelloyX substrates and corresponding reflection measurements. Even or odd higher-order interference peaks are selected by adjusting the optical thicknesses of the individual layers. The peak positions are very well reproduced by multiple-scattering calculations. With the HastelloyX substrate a potential application for high temperatures and aggressive atmospheres, e.g., in aircraft turbines, is addressed. A design for matching up to three turbine gas emission bands (CO_2, H_2O) is proposed.

1. Introduction

Multilayer stacks of at least two optically different materials – the one-dimensional version of photonic crystals [1] – can be designed, e.g. as reflective elements or as anti-reflection coatings by adjusting the thicknesses of the layers in the stack. For the reflective version with a stack of bilayers, the difference of the real part n of the refractive index of the two materials ("index contrast") should be as large as possible accompanied by low absorption, i.e. a small imaginary part k of the refractive index. When the bilayer thickness is about half the wavelength, constructive interference causes high reflectance. Mirrors on this basis have been reported from the microwave to the X-ray regime [2-10]. They can even form naturally as reported for ancient Roman glass [11].

The mirrors can exhibit a spectrum with either a broad reflection band or individual reflection peaks [4, 8, 12], making them useful for various applications. In the near infrared a potentially important application concerns aircraft turbines, where high temperatures lead to a strong radiative heat input from the hot gas into metallic structural components, e.g., the turbine rotor blades or stators. Coatings with increased reflectance can reduce the heat input, therefore contributing to a higher efficiency. In previous work, several stacks of multilayers with different layer thicknesses were typically used for this purpose, e.g., 12 stacks each with 12 bilayers for a broad wavelength band with about 90% reflectance between 1 and 5 μm [7, 8]. However, the hot turbine gas is characterized by an emission spectrum with peaks at characteristic wavelengths rather than by a continuous spectrum [13-16]. A mirror with specifically designed reflection peaks would then consist of stacks of multilayers with one stack for each emission band. Yet, a high number of individual layers with the corresponding need for high interface quality poses challenges for fabrication and selection of layer materials to minimize thermal stresses and to ensure excellent adhesion. Therefore, a reduction of the

number of layers would be highly desirable in terms of thermal and mechanical stability in a harsh environment at high temperatures and at varying operating conditions.

In this work, the basic and some application-related properties of *single-stack* multilayer mirrors are investigated, which are designed to exhibit a spectrum with multiple reflection peaks. For this single-stack design, a concept based on the selective generation of the multiple reflection peaks, i.e. higher-order interference peaks, is applied. For the near infrared (the main turbine gas emission regime) a numerical study as well as the experimental realization by the sputter deposition of multilayers and by corresponding reflection measurements are presented. In detail, the purpose of this investigation is to:

a) design *single-stack* multilayers with *several* reflection peaks, which are harmonics of the fundamental one. This is achieved by adjusting the optical thicknesses in the bilayers so that either even or odd higher harmonics are strongly enhanced (section 2). We note that the notation "higher harmonics" means higher-order interference, and should not be confused with similar notations in non-linear optics such as second harmonics generation.
b) determine the optical properties of the materials used (section 3) as input for the numerical calculations (section 2).
c) deposit TiO_2/Al_2O_3 multilayers as a model system on quasi-ideal (sapphire) and application-related substrates (HastelloyX) by sputtering (section 3.2).
d) perform reflection measurements of the multilayers in the near infrared (section 3.1) and compare the reflection spectra with the numerical results (section 4).
e) demonstrate, based on the reflection measurements, that a small number (5) of TiO_2/Al_2O_3 bilayers is already sufficient for strong higher order reflections (sections 4.1 - 4.3).
f) apply the results for matching the wavelengths of the main CO_2 and H_2O emission peaks in the near infrared in order to reduce radiative heat input into the substrate (section 4.4).

2. Selection of higher harmonics – the concept and the numerical method

The total reflectance of a multilayer stack is the result of multiple reflections at the interfaces and their interference. The individual layers in a bilayer have an optical thickness $d_{opt,i}$ depending on the geometrical thickness $d_{geo,i}$ and the real part n of the refractive index, $d_{opt,i} = n_i \cdot d_{geo,i}$ (i = TiO_2 or Al_2O_3 in this work). The concept of the selection of the higher harmonics is based on a proper variation of $d_{opt,i}$ and the interplay of destructive and constructive interference. At equal optical thickness of the two layers in the bilayer (50% of the optical thickness of the total bilayer, $d_{opt,tot}$), the reflections of the interfaces for the even harmonics of the fundamental (i.e. the 1st harmonic) interfere destructively. For the odd harmonics the interferences are constructive. This leads to the occurrence of odd higher harmonics beside the fundamental reflection. With deviations from 50% the condition for the destructive interference is no longer fulfilled and even harmonics appear. At a ratio of about 30%(TiO_2):70%(Al_2O_3) and vice versa, strong peaks of even harmonics dominate and largely destructive interference occurs for the odd higher harmonics (details in section 4.1). The exact positions of the harmonics depend on the geometrical thicknesses and on the variation of n of the two bilayer materials with the wavelength. Peak heights are determined by the index contrast and the number of bilayers.

For the implementation of this concept, calculations of the reflectance of the multilayers are performed by means of a multiple scattering method [17]. With this method multiple specular reflections at the interfaces are considered. In the software used in this work [18], non-ideal interfaces are considered by a roughness parameter σ according to Nevot and Croce [19, 20] and Vidal and Vincent [21]. σ is the root-mean-square roughness which can be interpreted as the width of a non-abrupt interface averaged over the various kinds of interface broadening (e.g. interdiffusion, lateral height variations). Not taking any details of the interface structure explicitly into account, the elements of the scattering transfer matrix are multiplied by factors

containing σ, which in turn reduces the reflectance of each interface. This results in the total reflectance being lower than without roughness.

For nearly ideal interfaces the roughness parameter σ is small compared to the bilayer thickness. For the multilayers deposited on sapphire for instance, σ is chosen to be 0.075 µm compared to approximately 1 µm bilayer thickness (details in section 4.2). For very rough interfaces, e.g. as a consequence of the multilayer deposition on 8% yttria stabilized zirconia (8YSZ) thermal barrier coating (TBC) on HastelloyX, a considerably larger value of σ has to be used. In this case diffuse scattering will likely also contribute to the reflectance which however cannot be considered by the multiple scattering method, as will be discussed in section 4.3.

3. Experimental methods and materials

3.1 Reflection and transmission measurements

The directional-hemispherical reflectance and transmittance of the samples prepared on transparent substrates are determined using a FTIR spectrometer with integrating sphere setup [22] and [23]. In the cases of the opaque HastelloyX and the multilayers on substrates only the reflectance is measured. With these setups spectral measurements are performed in the wavelength range from 1.6 µm to 25 µm at room temperature. In the following figures the data are shown up to shorter wavelengths as relevant for the present work. Figs. 1 and 3 concern the refractive index data of the single layers (TiO_2 and Al_2O_3), Figs. 5 – 8 the reflectance data of the multilayers.

The measured spectral reflectance and transmittance curves of the single layers on transparent sapphire substrates are analysed on the basis of the following formulae for a layer without diffuse scattering. This is considered as appropriate for the layers deposited homogeneously on the very smooth sapphire substrates. In this case the directional-directional reflectance ρ at the interfaces of two media with different complex refractive indices $m_1 = n_1 + ik_1$ and $m_2 = n_2 + ik_2$ as well as the directional-directional transmittance τ through the single layer with the complex refractive index $m_2 = n_2 + ik_2$ and the layer thickness d are given for perpendicular incidence by [24]:

$$\rho = \frac{[n_2 - n_1]^2 + [k_2 - k_1]^2}{[n_2 + n_1]^2 + [k_2 + k_1]^2} \tag{1}$$

$$\tau = \exp\left[-\frac{4\pi k_2}{\lambda} d\right] \ . \tag{2}$$

For a coating with two interfaces, the formulae for the directional-directional transmittance T_{dd} and reflectance R_{dd} are [24]:

$$T_{dd} = \tau \frac{[1-\rho]^2}{1-\rho^2\tau^2} \tag{3}$$

$$R_{dd} = \rho\left[1 + \frac{[1-\rho]^2\tau^2}{1-\rho^2\tau^2}\right] \tag{4}.$$

The measured spectral reflectance and transmittance curves of a single layer on a substrate were finally fitted by varying the complex refractive indices *m* in order to determine the real part *n* and the imaginary part *k* of the coating materials, which are needed for further analysis and modelling. The resulting relative uncertainty of the derived real part *n* and the imaginary part *k* of the coating materials is about ±5%.

For determining n and k of HastelloyX the fitting of the reflectance is performed including the Kramers-Kronig relations that relate n and k to each other allowing to determine both from the reflectance only.

3.2 Materials

TiO_2/Al_2O_3 multilayers as a model system were deposited on quasi-ideal single-crystalline sapphire substrates and on HastelloyX. The application to be discussed in section 4.4 will concern gas emissions as occurring in aircraft turbines. Therefore, HastelloyX (covered by a thermal barrier coating, TBC) as a standard nickel-based superalloy for turbine blades is used as a substrate.

3.2.1 Substrates

Sapphire is transparent in the relevant wavelength range from 1.6 µm – 7 µm [25]. For the deposition of single- and multi-layer coatings (0001) oriented single-crystalline sapphire substrate plates were used.

The HastelloyX substrate has specifications according to AMS 5536. The main constituents with typical percentages are Ni (47 wt%), Cr (22 wt%), Fe (20 wt%), Mo (9 wt%), and Co (1 wt%). The substrate is pre-coated with a NiCrAlY bond coating (Amdry 9624, thickness 200 µm) deposited by low vacuum plasma spraying and by a 8YSZ TBC (Metco 204NS, thickness 270 µm). The main constituents of the bond coating are Ni (66 wt%), Cr (22 wt%), Al (10 wt%), Y (1 wt%). 8YSZ (8 wt% yttria stabilized zirconium oxide), a frequently used TBC on nickel-based superalloys for high-temperature applications [26], is deposited by atmospheric plasma spraying showing the inherent characteristic pancake-like morphology [27].

The optical parameters n and k of uncoated HastelloyX for the near infrared wavelength range are not available in the literature. Therefore, they were deduced from reflection measurements conducted in this work (see section 3.1). The reflectance data shown in Fig. 1 are obtained after a heat treatment of HastelloyX at 1150°C which gives similar results at 1150°C and at room temperature.

Upon heat treatment the bond coating forms a thermally grown Al_2O_3 layer at the interface to the TBC (thickness approximately 5 µm). Our calculations showed that this layer has negligible effect on the reflectance and is therefore neglected. Since the remaining metallic part of the bond coating is a nickel-based alloy similar to the HastelloyX, it is optically included in the latter one.

The optical data for 8YSZ were taken from the literature, n from Nychka et al. [28] and k from Dombrovsky et al. [29]. n is approximately 2 in the relevant wavelength range up to 5 µm and decreases to 1.6 at 10 µm; k is negligibly small for $\lambda < 5$ µm. Above 5 µm k starts to increase, with the absorption still remaining weak up to about 7 µm.

The precoated HastelloyX substrates were ultrasonically cleaned in ethanol and dried, before they were mounted to the substrate holder. Prior to deposition of the TiO_2 and Al_2O_3 layers, the vacuum chamber was evacuated to a pressure $\leq 2\times10^{-5}$ mbar. Further substrate cleaning was done by Ar ion etching for 10 min, applying a pressure of 3×10^{-2} mbar and an asymmetrically bipolar pulsed d.c. voltage of -500 V at 50 kHz with a positive pulse of +37 V to avoid charging effects.

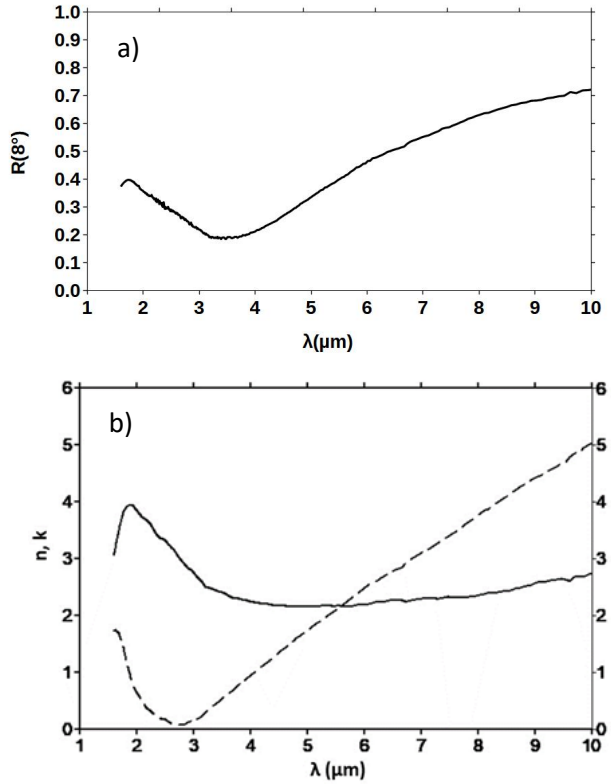

Fig. 1. a) reflectance R(8°) and b) real part n (full) and imaginary part k (dashed) of the refractive index of HastelloyX.

3.2.2 Single layer and multilayer coatings

Single TiO_2 and Al_2O_3 layers on sapphire for the determination of the refractive indices, as well as the TiO_2/Al_2O_3 multilayer stacks on sapphire and the HastelloyX substrates were deposited by magnetron sputtering. Consistently, Al_2O_3 was the first layer on the substrate and TiO_2 was the top layer. Magnetron sputter deposition represents a versatile method for the fabrication of high-quality layer materials with the required periodicity and sharp interfaces [30]. Due to the formation of strong interfaces between α-Al_2O_3 and rutile TiO_2 [31], strong interfacial adhesion can be expected.

The following aspects were considered for a successful deposition of the multilayers. Polymorphism of TiO_2 exists in the three crystalline forms anatase, rutile and brookite [32], where only rutile fulfils the criterion of the necessary thermal stability. Al_2O_3 forms beyond the stable α-Al_2O_3 also metastable phases like γ-Al_2O_3 or even amorphous phases, which can both be remarkably thermally stable up to temperatures >1000°C [33]. The Al_2O_3–TiO_2 phase diagram is characterized by low mutual solubility of Al_2O_3 in TiO_2 and vice versa [34], which guarantees high interfacial stability of TiO_2/Al_2O_3 multilayers. There is also only a small mismatch of thermal expansion of Al_2O_3 (α-Al_2O_3: 7.92×10^{-6} K^{-1} at 400°C and 9.22×10^{-6} K^{-1} at 1200°C [35]) and TiO2 (rutile: 6.99×10-6 K^{-1} (a-direction) and 9.37×10-6 K^{-1} (c-direction) at 25°C [36]), indicating low thermal stresses during thermal cycling of the multilayer stack.

For the magnetron sputter deposition, a custom-made laboratory-scale unbalanced pulsed d.c. system was used. The system was equipped with three 50.8-mm-diameter magnetron cathodes (AJA A320-XP) focused towards a rotating substrate holder. Coating deposition was

done using reactive d.c. magnetron sputtering of Al and Ti targets in an $Ar+O_2$ atmosphere. Sputtering of the targets was done in the current-controlled d.c. mode, with current set to 0.35 A for each target. For the Al_2O_3 layers, the total ($Ar+O_2$) pressure was 4.9×10^{-3} mbar and the O_2 partial pressure 1.4×10^{-3} mbar, whereas for TiO_2 the total pressure was set to 4.2×10^{-3} mbar and the O_2 partial pressure to 3.4×10^{-3} mbar. The substrate temperature and the rotation speed were set to 550°C and 50 rpm, while an asymmetrically pulsed d.c. voltage of -115 V (for the Al_2O_3 layer) or -50 V (for the TiO_2 layer), at 250 kHz, was applied to the substrate holder. For the deposition of the multilayers, sputtering of the respective targets was controlled via shutters.

Coating characterization was done by scanning electron microscopy (SEM) using a Tescan Clara field emission SEM, after metallographic preparation of cross-sections of the coated substrates. In addition to SEM, the thickness of the single layers was cross-checked by confocal laser microscopy (Keyence VK-X1100). Information about microstructure and chemical structure was obtained from X-ray diffraction (Bruker-AXS D8 Advance, Cu Kα radiation, voltage 40 kV, current 40 mA, step size 0.02°, time per step 1.2 s, glancing angle of 2°) and Raman spectroscopy (Witec alpha300R, laser wavelength of 532 nm, lateral resolution 900 nm).

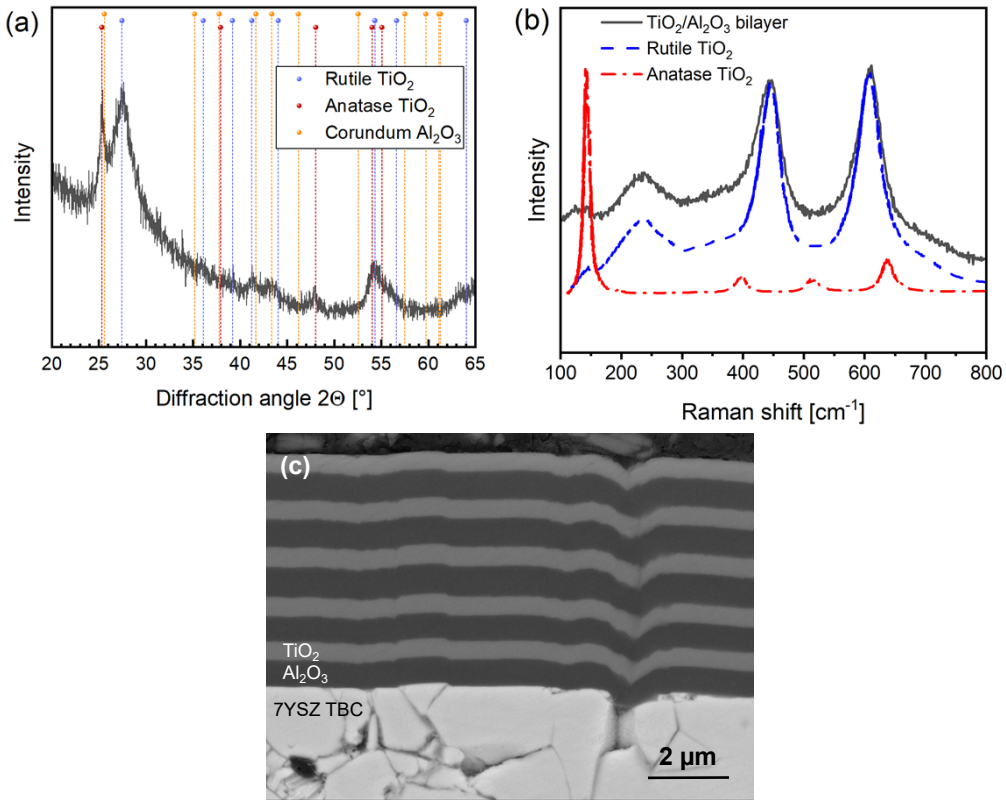

Fig. 2. Five bilayers TiO_2/Al_2O_3 stack deposited on 8YSZ precoated HastelloyX substrate. (a) Glancing angle X-ray diffractogram with the peak positions for rutile TiO_2, anatase TiO_2 and α-Al_2O_3 indicated (taken from [41]); (b) Raman spectrum of a metallographically prepared cross-section of the five bilayers stack (black line) with reference spectra for rutile (dashed blue line) and anatase TiO_2 (dash-dotted red line) taken from [37]; (c) Back-scattered electron SEM micrograph of a metallographically prepared cross-section.

Fig. 2 summarizes the results obtained for the fabricated samples consisting of five bilayers of TiO_2/Al_2O_3. The X-ray diffractogram in Fig. 2a clearly indicates the formation of rutile TiO_2;

however, it does not allow to unambiguously conclude about formation of anatase TiO_2 or crystalline Al_2O_3 phases. The Raman spectrum from the bilayers in Fig. 2b confirms formation of rutile without anatase (comparison with the RRUFF Raman database [37]), but no evidence for the formation of crystalline Al_2O_3 was found. This confirms earlier findings of largely amorphous Al_2O_3 coatings formed under the applied conditions [38]. Fig. 2c presents a SEM micrograph (back-scattered electrons) of the five bilayers TiO_2/Al_2O_3 on the 8YSZ precoated HastelloyX substrate, with the TiO_2 layers appearing bright and the Al_2O_3 layers appearing dark. The layer thickness is ~0.46 µm for TiO_2 and ~0.69 µm for Al_2O_3. It should be noted that the bilayer stack largely resembles the original roughness of the coarse-grained 8YSZ coating stemming from its characteristic pancake-like morphology, while the roughness is much less pronounced for the sapphire substrate leading to essentially plane-parallel interfaces. Film growth on the rough 8YSZ coating can be expected to cause local porosity due to atomic shadowing and the limited mobility of condensed atoms [39]. However, it is known that the density of the films increases with increasing film thickness [40], thus only a minor influence on diffuse scattering can be expected. Fig. 2c demonstrates that the porosity essentially appears in the TBC. Therefore, it is assumed that the optical properties of the materials in the bilayers are the same as those of the single layers (Fig. 3). We note that the YSZ TBC is intentionally porous to lower its thermal conductivity in turbine applications. Cracks that form during TBC application are intended to provide some strain tolerance and are highly needed.

Real and imaginary parts of the refractive index (n and k) of TiO_2 and Al_2O_3 were derived from transmission and reflection measurements of respective single layers on sapphire (thickness 1 – 2 µm). Results for the wavelength range between 1.6 µm and 10 µm are shown in Fig. 3. TiO_2 and Al_2O_3 fulfil the basic requirements of a large index contrast and low absorption in the near infrared. The index contrast is large for wavelengths below 7 µm and decreases rapidly above 7 µm where the imaginary part strongly increases. Therefore, the results presented in section 4.1 – 4.3 will cover only the wavelength range between 1.6 µm and 7 µm.

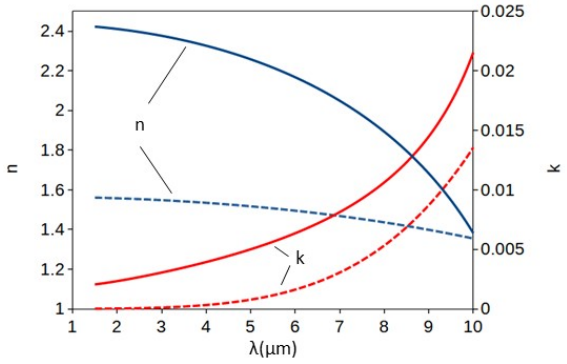

Fig. 3. Real parts n and imaginary parts k of the refractive index of TiO_2 (full) and Al_2O_3 (dashed).

TiO_2 exhibits one of the highest refractive index values ($n > 2$ in the wavelength range 1.6 – 7 µm) among the suitable materials. Replacing Al_2O_3 ($n \approx 1.5$) in the TiO_2/Al_2O_3 bilayer by a material with even lower n would increase the contrast. Examples are SiO_2 and halides like BaF_2, CaF_2, $CaCl_2$, and $BaCl_2$ ($n \approx 1.4$). However, crystalline SiO_2 has a phase transition at 573°C, which may cause high thermal stresses leading to delamination of the whole multilayer stack. Fluorides and chlorides pose huge difficulties for sputter deposition due to sputter targets being highly sensitive to moisture, corrosive and/or even toxic. Therefore, considering the only small gain in contrast, together with the requirements for the deposition of high-quality multilayer stacks and their application at high temperatures in aggressive atmospheres, Al_2O_3 appears to be the best suitable material for this study.

4. Results and Discussion

4.1 Basic numerical results

In order to investigate the general reflectance properties of multilayers designed according to the higher-harmonics concept in section 2, calculations with five bilayers TiO_2/Al_2O_3 without a substrate were performed in the wavelength range between 1 and 7 µm. The results are compiled in a colour plot (Fig. 4a) of the reflectance R as function of the wavelength λ (horizontal axis) and the relative optical thickness of the TiO_2 layer, $d^r_{opt}(TiO_2)$, given as the percent value of the total optical thickness of the bilayer $d_{opt,tot}$ (vertical axis). $d_{opt,tot}$ varies between 2.5 µm (at λ = 1 µm) and 2.1 µm (at λ = 7 µm) with maximal deviations of +/-0.1 µm for the different percent values of $d^r_{opt}(TiO_2)$. At λ= 2.8 µm $d_{opt,tot}$ is 2.4 µm for all the percent values.

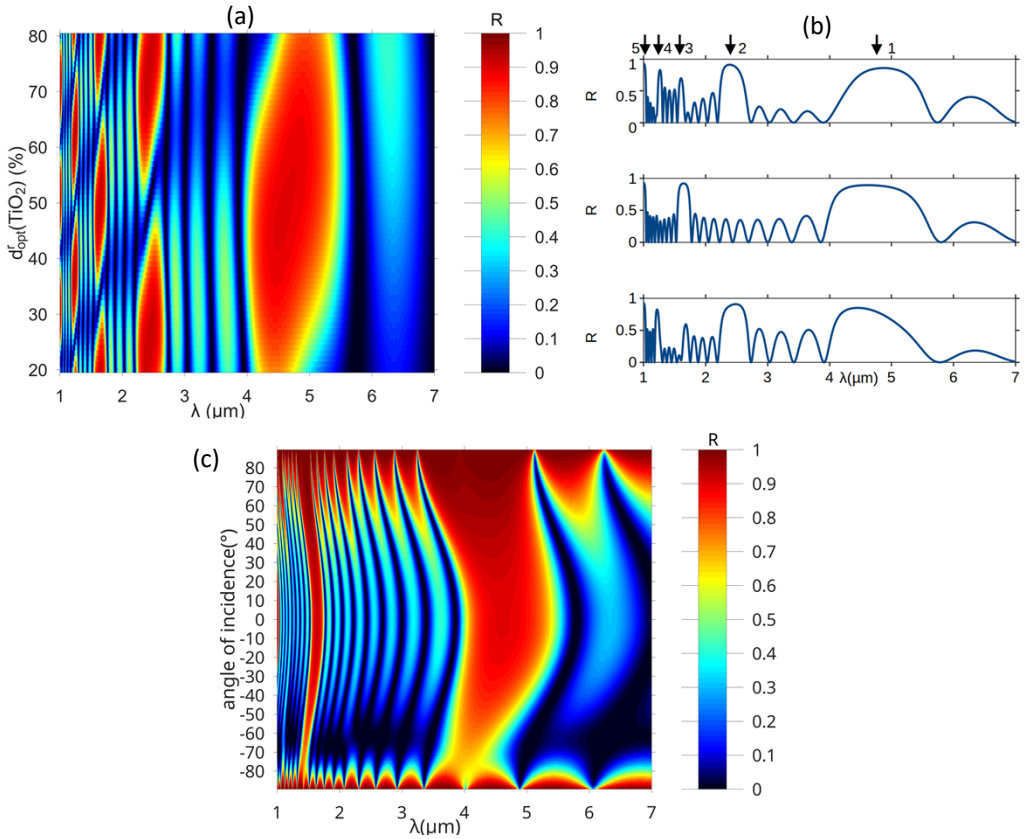

Fig. 4. a) Colour plot of the reflectance R vs. wavelength λ (horizontal axis) and relative optical thickness $d^r_{opt}(TiO_2)$ (vertical axis) for normal incidence. b) Reflectance spectra at constant $d^r_{opt}(TiO_2)$ = 30%, 50% and 70% (from bottom to top). Arrows indicate the positions of the harmonic peaks. c) Colour plot of the reflectance R vs. wavelength (horizontal axis) and angle of incidence (vertical axis) for $d^r_{opt}(TiO_2)$= 50%.

Horizontal cuts at different constant values of $d^r_{opt}(TiO_2)$ in Fig. 4a allow to select reflectance spectra with either even or odd higher harmonics or a mixture of both (Fig. 4b). The peak of the first harmonic occurs at 4.7 µm. The higher harmonics are approximately at wavelengths divided by a factor of 2, 3, 4, 5 etc., the exact positions being determined by the wavelength dependence of n. For $d^r_{opt}(TiO_2)$ = 50% (middle graph in Fig. 4b), the peak positions are λ ≈ 1.6 µm (3^{rd}), and λ ≈1 µm (5^{th}). As explained in section 2, the even harmonics are missing in this case, yet in a very narrow range of $d^r_{opt}(TiO_2)$ only. For $d^r_{opt}(TiO_2)$ = 30% (lower graph in Fig. 4b), the positions of the even harmonics are λ ≈ 2.4 µm (2^{nd}) and λ ≈ 1.25 µm (4^{th}). For 70% (upper graph in Fig. 4b), the spectrum is quite similar to the 30% case, yet the

peaks are shifted by a very small amount. $d^r_{opt}(TiO_2)$ = 30% (and 70%) were chosen to produce a strong 2nd harmonic peak without losing much reflectance of the 1st harmonic. In this case, also a weak peak of the 3rd harmonic appears in Fig. 4b, which would be essentially absent at 33 and 67% (see Fig. 4a). The 5th harmonic appears in all three spectra shown in Fig. 4b. The fine structure of the higher-harmonic peaks and their positions as function of $d^r_{opt}(TiO_2)$ in the colour plot are governed by several half wavelengths fitting into the bilayer. With increasing harmonic number, more changes between constructive and destructive interference as function of $d^r_{opt}(TiO_2)$ occur, clearly visible, e.g., for the 3rd and 4th harmonic at about 1.6 and 1.2 µm, respectively.

The dependence of the reflectance on incident angle is shown in Fig. 4c for s and p polarization by positive and negative angles, respectively. The angular dependence will be addressed in the discussion of the reflectance results in section 4.3.

4.2 Experimental realization of the concept for higher harmonics

Multilayers with five bilayers were deposited with the respective thickness of TiO_2 and Al_2O_3 chosen to result in a value of $d^r_{opt}(TiO_2)$ of either 30% or 50%, with the 1st harmonic peak nominally at 4.3 µm. Substrates were single-crystalline sapphire and HastelloyX pre-coated with 8YSZ-TBC as described in section 3.2.1. Due to several boundary conditions in the sputter deposition of the bilayer stacks, this nominal value of 4.3 µm may not be perfectly realized in all the samples. Therefore, for each measured spectrum separate calculations were performed in order to match the measured spectral positions of the 1st harmonic peak as good as possible.

Results of reflection measurements at room temperature and of calculations at 8° incident angle, R(8°), are shown for multilayers on sapphire substrates in Fig. 5 ($d^r_{opt}(TiO_2)$ = 30%) and Fig. 6 ($d^r_{opt}(TiO_2)$ = 50%). In the calculations, first the thicknesses were varied to give good agreement of the calculated with the experimental peak positions. To adjust the calculated peak heights and widths to the measured ones, the roughness parameter σ was varied. Best agreement for consistent heights was achieved with the calculated widths slightly smaller than in the experiment. For $d^r_{opt}(TiO_2)$ = 30% (Fig. 5), as expected from the calculation, a strong 2nd harmonic peak is observed experimentally. For nominally 50% (Fig. 6), the calculation gives the 3rd harmonic peak to be strong with the 2nd harmonic peak missing. The experimental 3rd harmonic peak at 1.6 µm is not entirely developed due to the restricted available wavelength range, but there is a clear indication for this peak. In addition, a smaller peak occurs at 2.5 µm, which is attributed to the 2nd harmonic appearing due to a deviation of $d^r_{opt}(TiO_2)$ from 50% in the deposited multilayers. The calculation with $d^r_{opt}(TiO_2)$= 46% gives indeed a weak peak at the position of the experimental peak.

We note that the oscillatory behaviour beside the harmonic reflection peaks is due to interference from the total thickness of the five bilayers, being essentially reproduced by the calculations. For instance, five oscillation peaks occur at wavelengths ranging from the 1st to the 2nd harmonic (including coincident peaks) so that three peaks are visible in between.

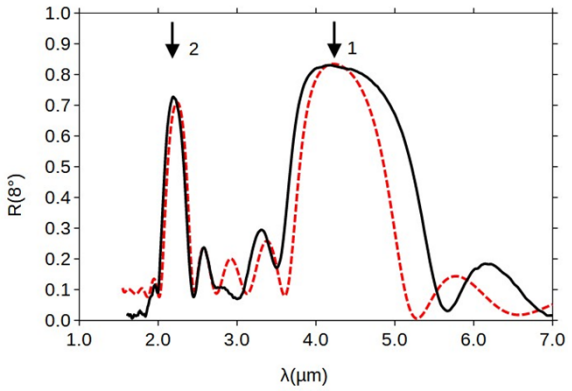

Fig. 5. Reflectance R(8°) of five bilayers TiO_2/Al_2O_3 on sapphire with the 1st and 2nd harmonic at λ= 4.2 and 2.2 μm, respectively, indicated by arrows. Experimental: full *(black)* curve. Calculation (dashed red curve): $d_{geo}(TiO_2)$ = 0.280 μm, $d_{geo}(Al_2O_3)$ = 0.992 μm, $d^r_{opt}(TiO_2)$ = 30%, σ = 0.075 μm.

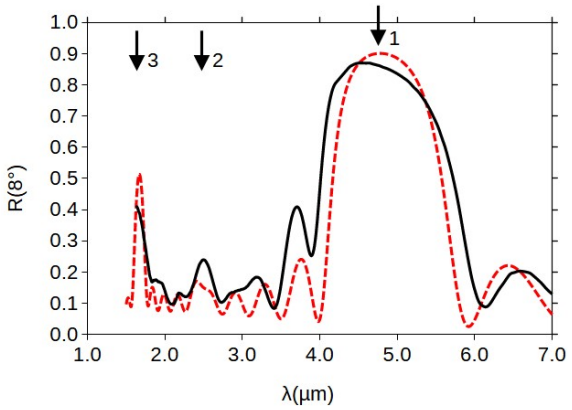

Fig. 6. Reflectance R(8°) of five bilayers TiO_2/Al_2O_3 on sapphire with the 1st and 3rd harmonic at λ= 4.7 and 1.6 μm, respectively (arrows). Experimental: full (black) curve. Calculation (dashed red curve): $d_{geo}(TiO_2)$ = 0.490 μm, $d_{geo}(Al_2O_3)$ = 0.844 μm, $d^r_{opt}(TiO_2)$ = 46%, σ = 0.075 μm. Details see text. The reflectance peaks are slightly shifted to higher wavelength compared to Fig. 5 because of larger layer thicknesses.

Corresponding results for reflection measurements on the 8YSZ-TBC/HastelloyX substrates with five TiO_2/Al_2O_3 bilayers at 8° incident angle are shown in Figs. 7 and 8 together with the respective calculations. The calculations give good agreement with regard to the peak positions. As expected from the higher-harmonics concept, reflection peaks of the 1st and 2nd harmonic are visible at 30% (Fig. 7) and of the 1st and 3rd harmonic at 50% (Fig. 8). The appearance of the 2nd harmonic peak at 2.3 μm for $d^r_{opt}(TiO_2)$ = 50% in the calculated spectra will be addressed in section 4.3.

Height and width of the measured peaks could however not be reproduced satisfactorily, even with a wide variation of the roughness parameter σ and a variation of $d^r_{opt}(TiO_2)$ around 30% and 50%, respectively. The most likely reason for these discrepancies is diffuse scattering as a consequence of the very rough surface (see Fig. 2c), as will be discussed in section 4.3. Diffuse scattering can also explain the strong damping of the oscillations beside the main reflection peaks.

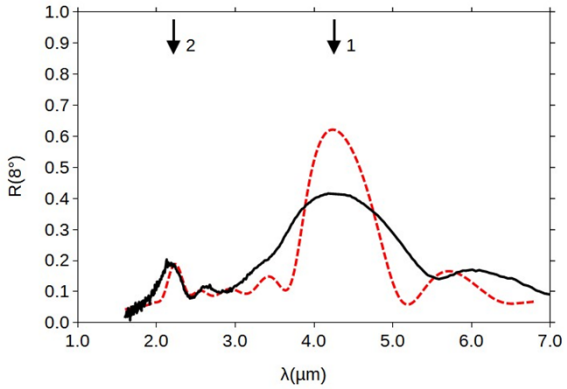

Fig. 7. Reflectance R(8°) of five bilayers TiO_2/Al_2O_3 on 8YSZ-TBC/HastelloyX substrate with the 1st and 2nd harmonic peaks at λ= 4.2 and 2.2 μm, respectively (arrows). Experiment: full black curve. Calculation (dashed red curve): $d_{geo}(TiO_2)$= 0.28 μm, $d_{sgeo}(Al_2O_3)$= 0.99 μm, $d^r_{opt}(TiO_2)$= 30%, σ= 0.15 μm.

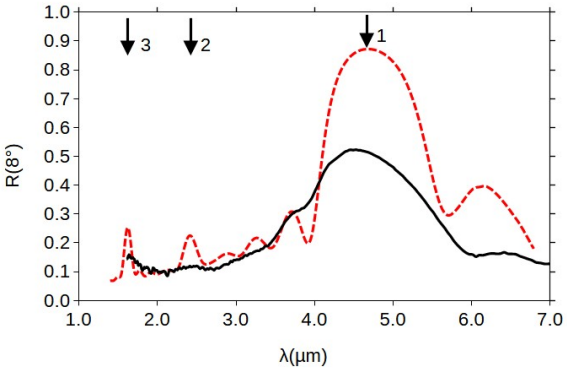

Fig. 8. Reflectance R(8°) of five bilayers TiO_2/Al_2O_3 on 8YSZ-TBC/HastelloyX substrate with the 1st harmonic at λ= 4.7 μm (arrow). Experiment: full black curve; the not fully developed peak at λ= 1.6 μm is at the position of the 3rd harmonic. Calculation (dashed red curve): $d_{geo}(TiO_2)$ = 0.50 μm, $d_{geo}(Al_2O_3)$ = 0.78 μm, $d^r_{opt}(TiO_2)$ = 50%, σ= 0.1 μm. Regarding the 2nd harmonic peak at λ= 2.3 μm see the discussion in section 4.3.

4.3 Discussion of the reflectance results

The most important general finding from Figs. 5 - 8 is that the higher-harmonics concept could be experimentally validated with multilayers deposited on different substrates. There is excellent agreement between calculated and measured reflectance spectra for quasi-ideal sapphire substrates. For a more application related substrate (YSZ-TBC/HastelloyX), there is good agreement of the peak positions but only qualitative agreement of the height and width of the reflectance peaks between experimental and calculated spectra. In the following the influence of interface roughness on the reflectance peak width and the occurrence of the 2nd and 3rd harmonic is discussed.

For the sapphire substrate, the width of the experimental peaks can be reproduced by the calculations when assuming a small interface roughness in the order of 10% of the layer thickness (Figs. 5 and 6). The roughness is considered in the program used for the calculations [18] by a Nevot-Croce factor (see section 2). Yet, for a very rough surface such as the 8YSZ-

TBC/HastelloyX substrate (see Fig. 2c) with a presumably strong contribution from diffuse scattering, this treatment is not appropriate. As an approach for estimating the effect of the diffuse scattering, the angular dependence of the reflectance (Fig. 4c) is considered. The pronounced angle dependence observed in the calculation is expected to result in a considerable broadening of the peaks as compared to the specular reflectance at a single angle. This agrees with the fact that experimental peaks are always broader than the calculated ones. A further but minor contribution to the deviations from the calculated results might come from the porosity of the YSZ-TBC. This could reduce the values of n and k as compared to the data taken from the literature for dense YSZ [31, 32].

For an ideal multilayer system (Fig. 4), there are certain $d^r_{opt}(TiO_2)$ values where either the 2nd or the 3rd harmonic perfectly interfere destructively. With rough interfaces the ideal interference conditions are somewhat disturbed. For instance, for $d^r_{opt}(TiO_2)$ = 50% (Fig. 8), the peak height of the 3rd harmonic (constructive interference) is reduced and the 2nd harmonic (destructive interference) appears. This behaviour is more strongly pronounced in the case of the 8YSZ-TBC/HastelloyX substrate with its high metallic reflectance. It is less pronounced in the case of the sapphire substrate since the reflectance at the Al_2O_3/sapphire interface is much weaker.

A detailed consideration of the diffuse scattering would need a structural model of the layers and the substrate as well as a numerical treatment beyond the multiple scattering method employed here. A suitable approach might be the finite-difference-time-domain (FDTD) method, where for a wave incident at a certain angle all the reflected waves are calculated [42]. Such a treatment is however out of the scope of the present work.

4.4 Multilayer design for matching CO_2 emission bands

The concept of the higher harmonics is now applied for modelling the reflectance spectra in a wavelength range, where emission bands of the hot gas in an aircraft turbine are expected. The purpose is to design the reflectance peaks as close as possible to the wavelengths of these bands, with the goal to eventually reduce the heat impact into combustion and turbine sections of aircraft engines. Unfortunately, emission spectra are not available in the open literature for these sections, but only for the exhaust plume. The result of a modelling procedure by Mahulikar et al. [13] is shown in Fig. 9a. The strongest emission band at 4.3 µm is assigned to CO_2 while both, CO_2 and H_2O, are expected to contribute to the 2.7 µm band. Finally, H_2O exhibits another broad double band around 6 µm. This assignment is supported by absorption measurements of CO_2 and H_2O in a gas cell [15], by a calculation of the absorption based on HITRAN data [43] as well as by measured gas emission spectra [14, 16].

As a model system for the calculation of the reflectance, again five bilayers of TiO_2/Al_2O_3 are used. For the high-temperature turbine application the substrate would be YSZ-TBC/HastelloyX (Fig. 9c), but results for the sapphire substrate are also shown (Fig. 9b). We applied the higher-harmonics concept by adjusting layer thicknesses and the optical thickness $d^r_{opt}(TiO_2)$. With the 1st and 2nd harmonics the emission peaks at 4.3 and 2.7 µm cannot be matched simultaneously because of too large spacing (compare Figs. 5-8). However, higher harmonics up to the 5th harmonic can be used (Fig. 9), whereby two different multilayer designs are considered for each of the substrates. For both designs the total optical thickness of the bilayer is the same and the 1st harmonic is at 13 µm wavelength (i.e. layer thicknesses considerable larger than in Figs. 5 – 8). The first design with $d^r_{opt}(TiO_2)$= 50% positions the 3rd and 5th harmonic peaks at the wavelengths of the 4.3 and 2.7 µm emission bands. For the second design with $d^r_{opt}(TiO_2)$= 25% also the 2nd harmonic peak is present and coincides with the 6-µm double band. $d_{geo}(TiO_2)$ and $d_{geo}(Al_2O_3)$ are 1.394 and 2.160 µm, respectively (first design), 0.697 and 3.240 µm, respectively (second design). For the "three-peak model" (2nd, 3rd and 5th harmonic), the peak heights are somewhat lower than for the first design, but still at an acceptably high level.

The differences between the results on the sapphire and YSZ-TBC/HastelloyX substrates are mainly due to the higher background reflectance and the lower peak values for the latter one. For the YSZ-TBC/HastelloyX the higher background is caused by its metallic reflectance and the lower peak values are due to the rougher surface with $\sigma = 0.05$ µm assumed here. Yet, this value is considerably smaller than the one used in Figs. 6 and 7, which requests for an improved interface quality.

These examples demonstrate clearly that the higher-harmonics concept for single-stack multilayers can be applied to create strong reflection peaks at two or even more wavelengths of interest. The ratio of the wavelengths is essentially fixed, but the positions can be adjusted by choosing the layer thicknesses and selecting different higher harmonics. A weak tuning is possible by varying d^r_{opt} of the individual layers (see high-R regions in Fig. 4).

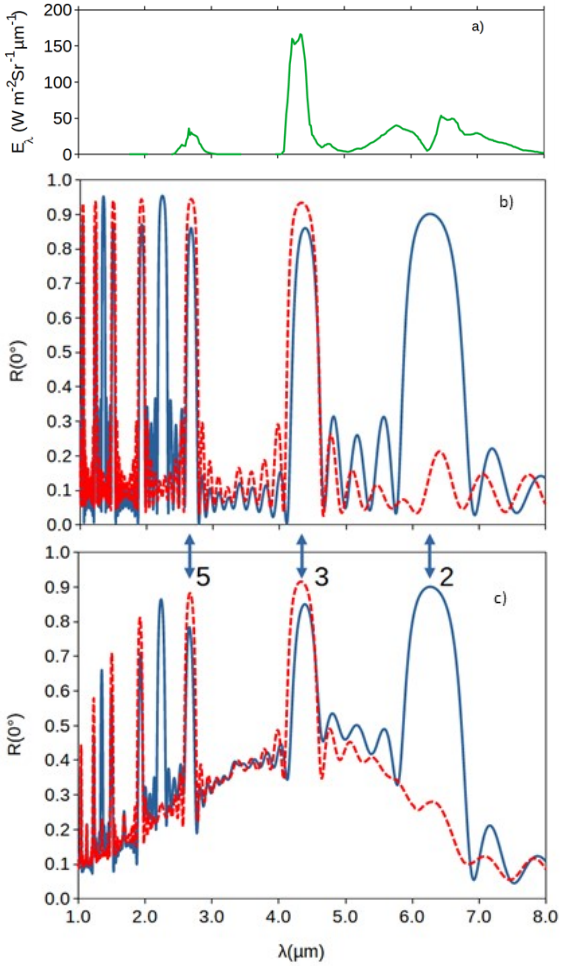

Fig. 9 a) Emission spectrum E_λ of hot turbine gas (figure adapted from [13]) and b,c) calculated reflectance spectra, R(0°), for two multilayer designs, $d^r_{opt}(TiO_2)$ = 50% (red, dashed) and 25% (blue, full); b) sapphire substrate, c) YSZ-TBC/HastelloyX substrate. For both designs the 3rd and 5th harmonic peaks are at λ= 4.3 and 2.7 µm, respectively. For 25% additionally the 2nd harmonic appears at λ= 6.3 µm.

5. Summary and Conclusions

5.1 Summary

We present a combined numerical and experimental investigation of the concept of multiple reflection peaks from single-stack multilayers by adjusting the strength of higher harmonics. A concept is presented which allows to design reflection spectra of multilayer mirrors where either even or odd higher harmonics of the fundamental (1st harmonic) dominate. This concept is validated experimentally by the fabrication of TiO_2/Al_2O_3 multilayers and measurements of corresponding reflection spectra in the near infrared. The positions of the reflectance peaks in the experimental spectra are in very good agreement with the calculated ones for multilayers on sapphire as well as on YSZ-TBC/Hastelloy substrates. Good agreement is obtained for the height and width of the peaks in the case of the sapphire substrate when assuming weak roughness (≈10%) of the interfaces. In the case of the YSZ-TBC/HastelloyX substrate with the coarse-grained structure of the TBC, the reflectance peaks are considerably broader than the calculated ones (even with high roughness), which is attributed to diffuse scattering. This indicates the limitations of the multiple scattering approach for the case of very rough interfaces. As an application example, the matching of emission bands of the hot gas in aircraft turbines by peaks in the reflectance spectrum is addressed numerically. Emission bands of CO_2 and H_2O at λ= 2.7, 4.3 and around 6 μm are well matched by using three higher harmonics with the fundamental one set at λ= 13 μm.

5.2 Conclusions

The higher-harmonics concept introduced in this work is appropriate for designing reflection peaks at distinct wavelengths where, beside the large index contrast, the two materials have weak absorption. The exact peak positions can be adjusted by the thickness of the individual layers and of the whole bilayer, where the positions are roughly proportional to the bilayer thickness. Either even or odd higher harmonics can be selected via the ratio of the optical thicknesses of the two individual layers.

Interface roughness influences the width of the reflectance peaks and weakens the strong distinction of even and odd higher harmonics. If this strong distinction is desirable (accompanied by high reflectance), smooth substrate surfaces and weak interface roughness in the multilayers have to be strived for.

The spacing of the peaks is variable by using either low-order or high-order harmonics. On the wavelength scale the low-order peaks are broader and more widely spaced than the high-order ones. An example is the possibility of choosing the 1st and 2nd harmonics or the 3rd and 5th harmonics. For instance, two emission bands of the hot gas in a turbine of an aircraft can be matched this way, and with the proper choice of $d^r_{opt}(TiO_2)$, even three emission bands can be covered with the 2nd, 3rd and 5th harmonics. This example was chosen to demonstrate the potential of reducing the radiative heat impact into turbine components, or alternatively to operate the turbine at a higher gas temperature. The selection of certain “harmonically-spaced” wavelengths out of a broad spectrum represents another potentially interesting application.

The substrates used in this work - sapphire and HastelloyX - are appropriate for investigating the basic properties of multilayer mirrors with high reflectance in the infrared and for high-temperature applications, respectively. The pancake-like structure of the YSZ-TBC on HastelloyX, however, has a restrictive effect for achieving high reflectance. Therefore, a smoother surface would be desirable. A first attempt to deposit the multilayers on polished TBC was not successful because of insufficient adhesion. A bonding layer as used between the Hastelloy and the TBC but of other architecture might avoid this problem.

The wavelength range studied is in the near infrared. An extension to the visible and near ultraviolet may work with the same multilayer materials down to about 0.3 μm. Magnetron sputter deposition is suitable to produce sufficiently sharp interfaces for the shorter wavelengths. Extension into the mid infrared beyond about 7 μm is difficult since TiO_2 and

Al_2O_3 show increasing absorption and reduced index contrast. A possible alternative to TiO_2 up to 10 µm would be HfO_2. Its real part of the refractive index is about 1.9 below 7 µm; it is 1.6 near 10 µm keeping the index contrast with Al_2O_3 higher than for TiO_2/Al_2O_3 at this wavelength (*cf.* Fig. 3). Wide-bandgap semiconductors like GaP with $n \approx 3.2$ in the wavelength range between 0.5 and 12 µm would give a very large index contrast but need a completely different deposition technique for single-crystal growth, e.g. chemical vapour deposition or molecular beam epitaxy.

5. Back Matter

Funding. This publication is based on experimental and partly on numerical work performed within the LuFo V-3 projects 20T1718A and 20T1718C funded by Deutsches Bundesministerium für Wirtschaft und Energie.

Acknowledgments. The authors are grateful to Velislava L. Terziyska, Dr. Anna Hofer-Roblyek and Gerhard Hawranek (all Montanuniversität Leoben) for their help with coating deposition and characterization.

Disclosures. The authors declare no conflicts of interest.

Data availability. Data underlying the results presented in this paper are not publicly available at this time but may be obtained from the authors upon reasonable request.

References

1. J. D. Joannopoulos, S. G. Johnson, J. N. Winn, *et al.*, "Photonic Crystals: Molding the Flow of Light," 2nd ed., Princeton University Press (2008).
2. D.A. Usanov, Nikitov, S.A., Skripal, *et al.*, "One-Dimensional Microwave Photonic Crystals - New Applications," 1st ed., CRC Press (2021).
3. F. Kuchar, R. Meisels, P. Oberhumer, *et al.*, "Microwave Studies of Photonic Crystals," Adv. Eng. Mater. **8**, 1156 - 1161 (2006).
4. D. E. Wolfe, J. Singh, R. A. Miller, *et al.*, "Tailored microstructure of EB-PVD 8YSZ thermal barrier coatings with low thermal conductivity and high thermal reflectivity for turbine applications," Surf. Coat. Technol. **190**, 132 – 149 (2005).
5. M. Campbell, D. N. Sharp, M. T. Harrison, *et al.*, "Fabrication of photonic crystals for the visible spectrum by holographic lithography," Nature **404** (6773), 53–56 (2000).
6. A. V. Vinogradov and B. Ya. Zeldovich, "X-ray and far uv multilayer mirrors: principles and possibilities," Appl. Opt. **16**, 89 – 93 (1977).
7. D. Wang, X. Huang, and P. C. Patnaik, "Design and Modeling of Multiple Layered TBC System With High Reflectance," J. Mater. Sci. **41**, 6245 – 6255 (2006).
8. X. Huang, "High Temperature Radiation Heat Transfer Performance of Thermal Barrier Coatings With Multiple Layered Structures," J. Eng. Gas Turbines Power **131**, 011301-1 – 011301-7 (2009).
9. Q. Huang, V. Medvedev, R. van de Kruijs, *et al.*, "Spectral tailoring of nanoscale EUV and soft x-ray multilayer optics," Appl. Phys. Rev. **4**(1), 011104 (2017).
10. R. Meisels and F. Kuchar, "Bragg mirrors with modified period for sub-10-nm wavelengths," OSA Continuum **4**, 2875 – 2891 (2021).
11. G. Guidetti, R. Zanini, G. Franceschin, *et al.*, "Photonic crystals built by time in ancient Roman glass," PNAS **120** (39), e2311583120 (2023).
12. Z. Wang and A. G. Michette, "Broadband multilayer mirrors for optimum use of soft x-ray source output," Journal of Optics A: Pure and Applied Optics **2,** 452 (2000).
13. S. P. Mahulikar, G. A. Rao, S. K. Sane, *et al.*, "Aircraft plume infrared signature in non-afterburning mode," J. Thermophys. Heat Transfer **19**, 413 – 415 (2005).
14. D. Marran, J. E. Cosgrove, J. Neira, *et al.*, "Turbine engine exhaust gas measurements using in-situ FT-IR emission/transmission spectroscopy," Proc. IEEE **4201**, 118 - 127 (2001).
15. M. Zipf, J. Manara, T. Stark, *et al.*, "Infrared-optical characterization of emitting and absorbing gases at high temperatures and high pressures," High Temperatures-High Pressures **47**(1), 3–21 (2018).
16. M. Paulec, M. Marciniak, K. Gross, *et al.*, "Infrared Signature Measurements of a Jet Turbine Using a Hyperspectral Imager for Combustion Diagnostics," Proc. SPIE **10644**, 106440W-1 - 106440W-11 (2018).
17. E. Centurioni, "Generalized matrix method for calculation of internal light energy flux in mixed coherent and incoherent multilayers", Appl. Opt. **44**, 7532 - 7539 (2005).
18. https://www.centu.it/optical. This is an up-dated version of the Centurioni program used in the present work. It includes roughness of the interfaces.
19. L. Nevot and P. Croce, "Caractérisation des surfaces par réflexion rasante de rayons X. Application à l'étude du polissage de quelques verres silicates," Rev. Phys. Appl. **15**, 761 - 779 (1980).

20. D. M. Smilgies, “Roughness in Specular Reflectivity,” https://www.classe.cornell.edu/~dms79/refl/XR-Roughness.html.
21. B. Vidal and P. Vincent, "Metallic multilayers for x rays using classical thin-film theory," Appl. Opt. **23**, 1794-1801 (1984).
22. L. Hanssen, “Integrating-sphere system and method for absolute measurement of transmittance, reflectance, and absorptance of specular samples,” Applied Optics **40,** 3196–3204 (2001).
23. J. Manara, M. Arduini-Schuster, and L. Hanssen, “Infrared-optical intercomparison measurements for evaluating the accuracies of the achieved results,” High Temp. – High Press. **38,** 259–276 (2009).
24. J. R. Siegel, J. Howell, and M. P. Mengüç, “Thermal Radiation Heat Transfer,” 3rd ed., CRC Press: Boca Raton, FL, USA (2011).
25. https://refractiveindex.info/?shelf=main&book=Al2O3&page=Querry-o. These are single-crystal data with n being about 0.15 higher than for the sputtered amorphous Al_2O_3 layer in Fig.3 which has a lower density.
26. J. L. Smialek and R. A. Miller, “Revisiting the Birth of 7YSZ Thermal Barrier Coatings: Stephan Stecura,” Coatings **8**, 255 (2018).
27. G. Bolelli, M. G. Righi, M. Z. Mughal, *et al.*, “Damage progression in thermal barrier coating systems during thermal cycling: A nano-mechanical assessment,” Materials and Design **166**, 107615 (2019).
28. J. A. Nychka, M. R. Winter, D. R. Clarke, *et al.*, “Temperature-Dependent Optical Reflectivity of Tetragonal-Prime Yttria-Stabilized Zirconia,” J. Am. Ceram. Soc. **89**, 908 - 913 (2006).
29. L. A. Dombrovsky, B. Rousseau, P. Echegut, *et al.*, “High temperature infrared properties of YSZ electrolyte ceramics for SOFCs: experimental determination and theoretical modeling,” J. Am. Ceram. Soc. **94**, 4310 – 4316 (2011).
30. R. Drevet, P. Souček, P. Mareš, *et al.*, “Multilayer thin films of aluminum oxide and tantalum oxide deposited by pulsed direct current magnetron sputtering for dielectric applications,” Vacuum 210, 111870 (2023).
31. M. N. Popov, J. Spitaler, M. Mühlbacher, *et al.*, “TiO2(100)/Al2O3(0001) interface: A first-principles study supported by experiment,” Phys. Rev. B **86**, 205309 (2012).
32. D. R. Eddy, M. D. Permana, L. K. Sakti, *et al.*, “Heterophase Polymorph of TiO_2 (Anatase, Rutile, Brookite, TiO_2 (B)) for Efficient Photocatalyst: Fabrication and Activity,” Nanomaterials **13**, 704 (2023).
33. F. Nahif, S. Mráz, D. Music, *et al.*, “Ab initio and experimental study on the effect of Y additions on the phase formation and thermal stability of Al_2O_3 thin films deposited by filtered cathodic arc evaporation,” Surf. Coat. Technol. **257**, 333-337 (2014).
34. In-Ho Jung, G. Eriksson, P. Wu, *et al.*, “Thermodynamic Modeling of the Al_2O_3–Ti_2O_3–TiO_2 System and Its Applications to the Fe–Al–Ti–O Inclusion Diagram,” ISIJ International 49, 1290-1297 (2009).
35. T. H. Nielsen and M. H. Leipold, “Thermal Expansion in Air of Ceramic Oxides to 2200°C,” J. Am. Ceram. Soc. 46, 381-387 (1963).
36. D. R. Hummer, P. J. Heaney, and J. E. Post, “Thermal expansion of anatase and rutile between 300 and 575 K using synchrotron powder X-ray diffraction,” Powder Diffraction **22**, 352-357 (2007).
37. RRUFF Raman Data Base, https://rruff.info
38. V. Edlmayr, M. Moser, C. Walter, *et al.,* “Thermal stability of sputtered Al_2O_3 coatings,” Surface and Coatings Technology **204,** 1576-1581 (2010).
39. C-C. Lai, R. Boyd, P-O. Svensson, *et al.*, “Effect of substrate roughness and material selection on the microstructure of sputtering deposited boron carbide thin films,” Surface and Coatings Technology, 433, 128160 (2022).
40. M. Ohring, “Materials Science of Thin Films - Deposition and Structure,” 2nd ed., Academic Press (2002).
41. International Center for Diffraction Data, PDF-2/Release 2007, https://www.icdd.com/
42. A. Taflove, “Computational Electrodynamics: The Finite-Difference Time-Domain Method,” Artech House, Boston and London (2005).
43. HITRAN - high-resolution transmission molecular absorption database, https://hitran.org/.